J. Am. Soc. Mass Spectrom. (2018) 29:2341–2359
DOI: 10.1007/s13361-018-2052-5

RESEARCH ARTICLE

Protonated Asparaginyl-Alanine Decomposition: a TCID, SORI-CID, and Computational Analysis

Georgia C. Boles,[1] R. R. Wu,[2] M. T. Rodgers,[2] P. B. Armentrout[1]

[1]Department of Chemistry, University of Utah, 315 S. 1400 E. Rm. 2020, Salt Lake City, UT 84112, USA
[2]Department of Chemistry, Wayne State University, Detroit, MI 48202, USA

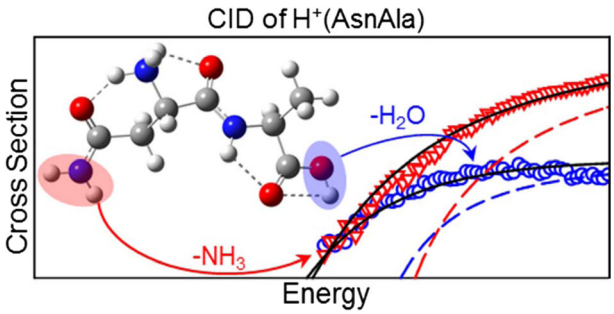

Abstract. Deamidation of asparagine residues, one of the fastest known post-translational modifications in proteins, plays a significant role in various biological functions and degenerative, aging diseases. Here, we present a full description of deamidation (as well as other key dissociation processes) from protonated asparaginyl-alanine, H^+(AsnAla), by studying its kinetic energy-dependent threshold collision-induced dissociation (TCID) with Xe using a guided ion beam tandem mass spectrometer. Relative thresholds compare favorably with those acquired by sustained off-resonance irradiation-CID of H^+(AsnAla) with Ar in a Fourier transform ion cyclotron resonance mass spectrometer. Absolute threshold energies from the TCID studies are compared to relative single point energies of major reaction species calculated at the B3LYP, B3LYP-GD3BJ, B3P86, MP2(full), and M06-2X levels of theory. Relative energies of key TSs and products allow for the characterization of the important rate-limiting steps involved in H^+(AsnAla) decomposition. The influence of water solvation on key TSs is also explored computationally, where bridging the gap between gas-phase and solvated studies is an important aspect of the biological relevance of this analysis. The comprehensive results presented (in addition to complementary studies discussed herein) allow for an insightful comparison to previous deamidation studies such that effects of the C-terminal residue side chain can be elucidated.

Keywords: Protonated peptide, Deamidation, Reaction mechanisms, Energetics, Thermodynamics

Received: 3 July 2018/Revised: 6 August 2018/Accepted: 6 August 2018/Published Online: 29 August 2018

Introduction

Under physiological conditions, peptides and proteins are susceptible to various chemical modifications [1]. Of these, post-translational modifications (PTMs) are particularly frequent and play an important role in protein and cellular function [1], metabolism [2], and signal transduction [3]. One of the fastest known PTMs involves the spontaneous deamidation of asparaginyl (Asn) residues [4]. Here, amide functionality is lost via the removal of ammonia, where a succinimide product is most commonly formed under physiological conditions [4], Scheme 1. Although deamidation has been associated with several regulatory functions (acting as a "molecular clock"), deamidation at asparaginyl residues is also a primary route of protein degradation, with rates that vary over three orders of magnitude as the adjacent C-terminal residue side chain is altered [4]. Succinimide intermediates readily undergo hydrolysis under aqueous conditions, producing a combination of iso-aspartate (iso-Asp) and aspartate (Asp) [4], Scheme 1, where the production of iso-Asp (which introduces an extra carbon to the backbone of the protein) has been linked to the onset and progression of degenerative aging diseases [5]. Under gas-phase conditions, succinimide transformation to these Asp and iso-Asp residues is negated, allowing for the determination of factors that control succinimide formation exclusively. Thus, the gas-phase evaluation of deamidation processes (and specifically succinimide formation) is of great interest and determining the specific

Electronic supplementary material The online version of this article (https://doi.org/10.1007/s13361-018-2052-5) contains supplementary material, which is available to authorized users.

Correspondence to: P. B. Armentrout; *e-mail:* armentrout@chem.utah.edu

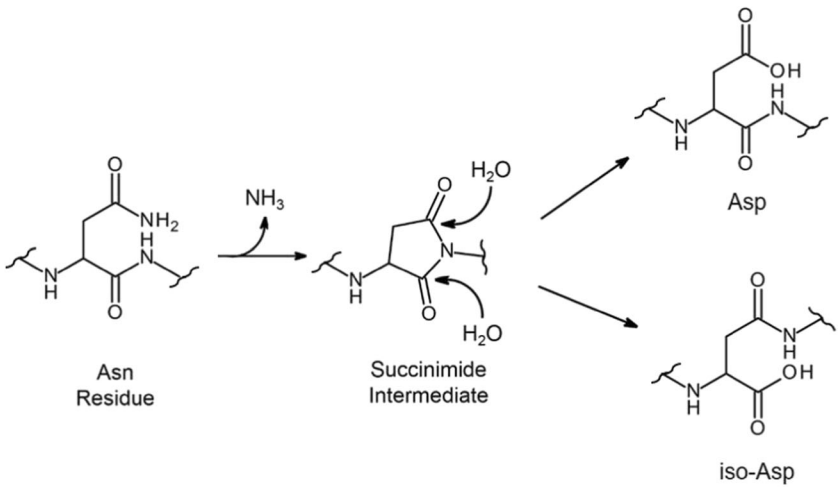

Scheme 1. Deamidation of asparagine residues in peptides leads to succinimide intermediates that can be hydrolyzed to form both Asp and iso-Asp residues under physiological conditions

interactions that play a significant role in hindering or accelerating the deamidation process is particularly important. Intriguingly, the solution-phase deamidation process is very sensitive to C-terminal residue side-chain effects, e.g., $n + 1$ residues of Gly, Ala, and Val have deamidation rates of about 1, 25, and 253 days [6].

In the current work, we examine the deamidation of protonated asparaginyl-alanine, H^+(AsnAla), using two gas-phase experimental techniques. Such analyses allow for the evaluation of adjacent C-terminal residue side-chain effects via comparison to our previous studies of H^+(AsnGly) [7] and H^+(AsnVal) [8]. The systematic analysis of these aliphatic C-terminal residue side chains allows for the determination of $n + 1$ residue steric effects with regard to product ion formation and reaction energetics. This provides the foundation for more detailed analyses of functionalized side chains, such as threonine and serine, where similar steric but differing inductive and electrostatic effects may become important, work currently underway in our laboratory. The major reactions observed in these studies are deamidation and dehydration. Threshold collision-induced dissociation (TCID), a technique allowing accurate determination of thermochemistry, was carried out in a guided ion beam tandem mass spectrometer (GIBMS). These results are compared to those obtained via sustained off-resonance irradiation (SORI)-CID, carried out in a Fourier transform ion cyclotron resonance mass spectrometer (FT-ICR MS), a technique commonly used for dissociating large biological molecules with high resolution and mass accuracy. Because quantitatively determining the internal energy resulting from SORI collisions is difficult (a result of the oscillating nature of the kinetic energy as well as the multiple collision activation) [9, 10], SORI-CID data are used here to verify adequate mass separation between nearby products and to provide a qualitative comparison to kinetic energy-dependent cross sections obtained via TCID studies. Comparison of these results provides valuable information regarding how deamidation (and other dissociation processes) are affected by different collision conditions and reaction times. Reaction energies reported are obtained from analysis of TCID thresholds and compared to theoretical results calculated at the B3LYP, B3LYP-GD3BJ, B3P86, MP2(full), and M06-2X levels of theory using a 6-311+G(2d,2p) basis set. Additionally, product ion formation determined from these theoretical results are compared to dehydration and deamidation products observed previously in infrared multiple photon dissociation (IRMPD) spectroscopy studies of H^+(AsnAla) [11]. This comprehensive analysis (including discussion of relevant literature) allows for a complete evaluation of the important dissociation pathways of H^+(AsnAla), which provides fundamental information regarding the specific intramolecular interactions that play significant roles in the deamidation process as well as other fragmentations.

Experimental and Computational Methods

General Experimental Procedures—GIBMS

Kinetic energy-dependent cross sections for the CID of H^+(AsnAla) with Xe were measured using a GIBMS (Armentrout Laboratory, U. Utah) that has been described in detail elsewhere [12–14]. Briefly, ions were generated using an electrospray ionization (ESI) source [15] under similar conditions to those described previously. The ESI was operated using 5×10^{-5} M AsnAla (purchased from AnaSpec, Fremont, CA, USA) in 50:50 (by volume) MeOH:H_2O solution, acidified with 0.1% acetic acid (purchased from Sigma-Aldrich, St. Louis, MO, USA), and directly infused using a syringe pump at a rate of 50 μL/h into a 35 gauge stainless steel needle biased at 2200–2400 V relative to ground. Ions were directed through a heated capillary at 80 °C into a radio frequency (rf) ion funnel [16], where they were focused into a tight beam. After exiting the ion funnel, the ions entered a rf trapping hexapole ion guide where

the ions underwent on the order of 10^4 thermalizing collisions with ambient gas. As demonstrated in earlier studies, ions produced in the source region should have a Maxwell-Boltzmann distribution of rovibrational states at 300 K [15, 17–20].

The precursor H^+(AsnAla) ions were extracted from the source, mass selected using a magnetic momentum analyzer, decelerated to a well-defined kinetic energy, and focused into an rf octopole ion guide that trapped the ions radially [12, 21, 22], which minimizes losses of product and reactant ions. The octopole passes through a collision cell containing xenon [23, 24] at a sufficiently low pressure (< 0.4 mTorr) such that the opportunity for multiple collisions to occur was minimal, although the number of ions undergoing single collisions was sufficient to yield good signal-to-noise in the product cross sections. The product and residual reactant ions drifted to the end of the octopole guide, where they were extracted and focused into a quadrupole mass filter for mass analysis. Ions were detected with a high voltage dynode and scintillation detector [25], and the signal was processed using standard pulse counting techniques.

Ion intensities of reactants and products, measured as a function of collision energy, were converted to absolute cross sections as described previously [12]. Briefly, the calculation of the total cross section (σ_{tot}) from the ion intensities utilizes a relationship that is directly analogous to the Beer-Lambert Law, specifically, $I = I_0\ exp(-\rho\sigma_{tot}l)$, where I is the reactant ion intensity after passing through the collision cell, I_0 is the reactant ion intensity entering the collision cell which equals $I + \sum I_j$ (where I_j = intensity of the product ion for channel j), l is the effective length of the collision cell (8.3 cm), and ρ is the number density of the neutral reactant and equals P/k_BT, where P and T are the pressure and temperature of the gas and k_B is Boltzmann's constant. Reaction cross sections for individual product ions are given by $\sigma_j = \sigma_{tot}\ (I_j/\sum I_j)$. The uncertainty in these relative cross sections is about ± 5% and that for the absolute cross sections is about ± 20% [12]. The ion kinetic energy distribution was measured using a retarding potential analysis [12] and found to be Gaussian with a typical full width at half maximum (FWHM) of 0.1–0.2 eV (lab). Ion kinetic energies in the laboratory (lab) frame were converted to energies in the center-of-mass (CM) frame using $E_{CM} = E_{lab} \times m/(m + M)$, where M and m are the masses of the ionic and neutral reactants, respectively. Uncertainties in the absolute energy scale are about ± 0.05 eV (lab) or ± 0.02 eV (CM). All energies below are reported in the CM frame.

General Experimental Procedures—SORI-CID

A Bruker 7T SolariX Hybrid FTMS mass spectrometer (Q-FT-ICR MS) (Rodgers Laboratory, Wayne State University) was used to perform the SORI-CID of H^+(AsnAla). The AsnAla dipeptide was synthesized, purified, and provided by the Polfer Laboratory of the University of Florida. (A different supplier of the AsnAla sample was used in the GIBMS experiments because they were performed much later than the FT-ICR experiments and we wanted to ensure that the samples had not degraded, presumably by deamidation.) A 0.1 mM solution of H^+(AsnAla) was prepared by dissolving an appropriate amount of AsnAla in a 50:50 MeOH:H_2O solution with a total concentration of 1% acetic acid. The solution was delivered to the ESI source at a flow rate of 2.0 μL/min. The ions passed through a glass capillary, were orthogonally extracted into a dual ion funnel, decelerated, and cooled within the source multipole, and focused and guided through a quadrupole mass filter for mass-selection. The mass-isolated H^+(AsnAla) ions were directed by a rf hexapole ion guide through the inhomogeneous fringing field of the superconducting magnet into the ICR cell. Argon gas was pulsed into the cell to induce SORI-CID fragmentation of the H^+(AsnAla) ions. The SORI power was gradually increased from 0.0 to 0.5% at a step size of 0.05%, and from 0.5 to 0.8% at a step size of 0.1%, with an irradiation time of 0.5 s at each step. Multiple collision conditions dominate in these experiments.

Thermochemical Analysis

Thresholds of TCID cross sections for fragmentation channel j were modeled using Eq. 1,

$$\sigma_j(E) = \left(n\sigma_{0,j}/E\right)\sum_i g_i \int_{E_{0,j}-E_i}^{E} \left[k_j(E^*)/k_{tot}(E^*)\right]\left\{1-e^{-k_{tot}(E^*)\tau}\right\}(E-\varepsilon)^{n-1}d(\varepsilon) \quad (1)$$

where $\sigma_{0,j}$ is an energy-independent scaling factor for channel j, n is an adjustable, empirical representation of factors that describe the efficiency of the energy transfer during collision and varies with the complexity of the system being studied [13], E is the relative kinetic energy of the reactants, $E_{0,j}$ is the threshold for dissociation of the ground electronic and rovibrational state of the reactant ion at 0 K into channel j, τ is the experimental time for dissociation (~5×10^{-4} s, as measured by previous time-of-flight studies [13]), ε is the energy transferred from translation to internal modes during the collision, and E^* is the internal energy of the energized molecule (EM) after the collision, so that $E^* = \varepsilon + E_i$. The summation is over the rovibrational states of the reactant ions, i, where E_i is the excitation energy of each state and g_i is the fractional population of those states ($\Sigma g_i = 1$). The Beyer-Swinehart-Stein-Rabinovitch algorithm [26–28] was used to evaluate the number and density of the rovibrational states and the relative populations g_i were calculated for a Maxwell-Boltzmann distribution at 300 K. The term k_j (E^*) is the unimolecular rate constant for dissociation of the EM to channel j via its rate-limiting transition state (TS). The rate coefficients k_j (E^*) and k_{tot} (E^*) are defined by Rice-Ramsperger Kassel-Marcus (RRKM) theory as in Eq. 2 [29, 30],

$$k_{tot}(E^*) = \sum_j k_j(E^*) = \sum_j s_j N_j^{\dagger}(E^* - E_{0,j})/h\rho(E^*) \quad (2)$$

where s_j is the reaction degeneracy of channel j, $N_j^{\dagger}(E^* - E_{0,j})$ is the sum of rovibrational states for the TS of channel j at an energy $E^* - E_{0,j}$, h is Planck's constant, and $\rho(E^*)$ is the density of states of the EM at the available energy, E^*. These rate

coefficients allow both kinetic shifts (where the probability of dissociation is given by the term $P_D = \left\{1-e^{-k_{tot}(E^*)\tau}\right\}$ in Eq. 1) and competition between multiple channels (which is controlled by the ratio of rate coefficients in Eq. 1, $[k_f(E^*)/k_{tot}(E^*)]$) to be modeled accurately [31, 32].

The decomposition of H^+(AsnAla) also involves a sequential dissociation process where modeling of this channel requires additional constraints [33]. Here, the initial dissociation takes away an unknown distribution of energy in translational modes of the primary products as well as in internal modes of the neutral product. Thus, the probability of the primary ion product undergoing further dissociation is $P_{D2} = \left\{1-e^{-k_{2tot}\left(E_2^*\right)\tau_2}\right\}$, where k_{2tot}, E_2^*, and τ_2 are the total rate coefficient for secondary dissociation, the internal energy available to the primary product ion (the secondary energized molecule, EM_2), and the time available for the second dissociation, respectively. For these processes, the CID cross section for a particular channel j (Eq. 1) is partitioned into a cross section for non-dissociating products, $\sigma_{ND}(E) = \sigma_j(E)(1 - P_{D2})$, and one for the sequential dissociation product ion, $\sigma_D(E) = \sigma_j(E) P_{D2}$. Rate coefficients k_{2tot} for EM_2 are again calculated using RRKM theory, Eq. 2. The energy available to EM_2 is defined statistically, as detailed elsewhere [33].

Several effects complicate the data analysis and must be accounted for to produce accurate thermodynamic information. First, the kinetic energy distributions of the reactants result in energy broadening, which is accounted for by explicit convolution of the model over kinetic energy distributions of both reactants, as described elsewhere [12]. After this convolution, the threshold model of Eq. 1 includes all sources of energy available to the reactants. The second effect involves the necessity of single-collision events in order for the energy deposition to be accurately modeled using Eq. 1. To ensure single-collision conditions, data for the high mass-resolution conditions were collected at three pressures of Xe, here about 0.3, 0.2, and 0.1 mTorr, and the resulting cross sections evaluated for pressure effects and extrapolated to zero pressure when pressure effects outside the range of experimental error were detected [34]. The last effect arises from the average lifetime for dissociation, which can result in a kinetic shift of the CID threshold and increases as the size of the molecule increases. To estimate the kinetic shifts observed, the thresholds were also determined without including RRKM modeling ($P_D = 1$) and competition in Eq. 1.

To evaluate the rate coefficients in Eqs. 1 and 2, the needed sets of rovibrational frequencies for the EM and rate-limiting TSs were determined from quantum chemical calculations as discussed in the following section. The entropy of activation at 1000 K for each dissociation channel was calculated as described in detail elsewhere [32]. The model cross sections of Eq. 1 were convoluted with the kinetic energy distributions of the reactants [12] and compared to the experimental data. A nonlinear least-squares analysis was used to determine optimized values for $\sigma_{0,j}$, n, and $E_{0,j}$. The uncertainty in $E_{0,j}$ (one standard deviation) was estimated from the range of threshold values determined from multiple sets of data, variations in the parameter n (± 10% around the optimum value), variations in vibrational frequencies (± 10%), changes in τ by factors of 2, and the uncertainty in the absolute energy scale (0.02 eV).

Computational Details

Structures, vibrational frequencies, and energetics for all species were calculated using the Gaussian 09 suite of programs [35]. To ensure that the ground structures (GS) of reactant and product species were correctly identified, structures previously reported for H^+(AsnGly) [7] were used as starting structures, where a methyl group replaced one of the hydrogens of the C-terminal residue side chain while ensuring L stereochemistry was maintained. Optimizations of all unique low-energy structures were conducted at the B3LYP/6-311+G(d,p) level of theory. Starting structures for additional key reaction intermediates and all TSs were also initially taken from the resulting structures reported for our H^+(AsnGly) study. These structures were further optimized at the B3LYP, B3LYP-GD3BJ, and M06-2X levels of theory with a 6-311+G(d,p) basis set. Each TS was verified to contain a single imaginary frequency, and it was determined that each intermediate was vibrationally stable.

Rotational constants and vibrational frequencies were calculated from optimized structures, and vibrational frequencies were scaled by a factor of 0.989 [36] when used for the determination of internal energy, RRKM calculations, and zero-point vibrational energy (ZPE) corrections. Single point energies of all species were calculated using the 6-311+G(2d,2p) basis set at the B3LYP, B3P86, and MP2 (full) levels using B3LYP geometries, and also at the B3LYP-GD3BJ/6-311+G(2d,2p)//B3LYP-GD3BJ/6-311+G(d,p) and M06-2X/6-311+G(2d,2p)//M06-2X/6-311+G(d,p) levels. Below, these results are referred to simply as B3LYP, B3P86, MP2, B3LYP-GD3BJ, and M06-2X, respectively. Studies of amino acid systems of similar composition have shown that B3LYP-GD3BJ empirical dispersion corrections better describe the hydrogen bonding in these systems [37]. Conversion from 0 to 298 K reaction enthalpies and Gibbs energies was accomplished using the rigid rotor/harmonic oscillator approximation with rotational constants and vibrational frequencies calculated at the B3LYP/6-311+G(d,p) level.

Results

Cross Sections for Collision-Induced Dissociation—GIBMS

Experimentally determined kinetic energy-dependent cross sections were obtained for the interaction of Xe and H^+(AsnAla) ($m/z = 204$). High mass-resolution conditions were used to allow characterization of cross sections for channels separated by 1 amu. As discussed previously [7], a lower pole

offset voltage on the quadrupole mass filter is required to obtain high mass-resolution conditions, which limits the energy range over which ions are efficiently transmitted in the laboratory frame. Figure 1 shows a representative dataset taken at 0.3 mTorr of Xe. As defined further below, *m/z* 186 (dehydration) and 187 (deamidation) appear competitively with apparent thresholds near 1 eV. Dehydration has the lower threshold, although deamidation dominates the dehydration channel at higher energies. At collision energies about one electron volt higher, the formation of *m/z* 170 and 87 occur competitively. At even higher energies, the formation of *m/z* 115, 124, 145, and 158 is observed.

On the basis of the computed reaction pathways described further below, Scheme 2 suggests there are five primary channels in the decomposition of H^+(AsnAla). In addition to the dominant deamidation and dehydration channels, H^+(AsnAla) also decomposes by cleavage of the peptide bond, eliminating alanine (Ala) with and without concomitant CO loss to form *m/z* 87 and 115, respectively. The latter product might also decarbonylate yielding *m/z* 87 at higher energies. The final primary dissociation is loss of the carboxamide side chain from H^+(AsnAla), which leads to *m/z* 145. At higher energies, the primary deamidation product undergoes sequential dissociation by losing another NH_3 molecule resulting in *m/z* 170, which can lose CO and H_2O yielding *m/z* 124. The primary dehydration product can also decarbonylate to form *m/z* 158. Conceivably, this product could lose two ammonia molecules yielding *m/z* 124, although the intermediate *m/z* 141 is not observed.

Scheme 2 identifies one possibility for *m/z* 187 as protonated 3-amino-N-2-methyl ethanoic acid-succinimide, H^+(AMEA-Suc). Its secondary NH_3 loss product is identified as protonated 2-oxo-3N-vinyl ketone-4-methyl oxazolone, H^+(OVK-Oxa). Alternatively, deamidation of similar systems [8, 11] has revealed that furanone moieties can also be formed such that Scheme 2 includes this alternate structure, 4-amino,5-2-λ^2-methyl-azanylacetic acid 3H-furan-2-one, H^+(AMA-Fur). Its secondary NH_3 loss removes the amino group to yield H^+(MA-Fur). Dehydration of H^+(AsnAla) is proposed to yield an oxazolone structure, specifically 2-(3-aminopropanamide)-5-(4H,4-methyl)-oxazolone, H^+(APAM-Oxa), as is typical for such a b_2 ion [38–40]. Likewise, the *m/z* 145, 115, and 87 products are identified as protonated glycyl-alanine, H^+(GlyAla), protonated amino furanone, H^+(A-Fur), and protonated 3-aminopropanamide, H^+(APA), respectively.

Collision-Induced Dissociation—SORI

Figure 2 shows the SORI-CID of H^+(AsnAla), which resulted in major products at *m/z* 187, 186, 170, 169, 158, and 124. As mentioned above, the power dependence of SORI data cannot be interpreted quantitatively, although comparison with the TCID results confirms several aspects of the qualitative behavior of the observed cross sections. Specifically, the deamidation and dehydration channels have similar low-energy thresholds and magnitudes that favor *m/z* 186 at low energies and *m/z* 187 at high energies. In addition, the sequential channel *m/z* 170 is consistent with the TCID results regarding its relative

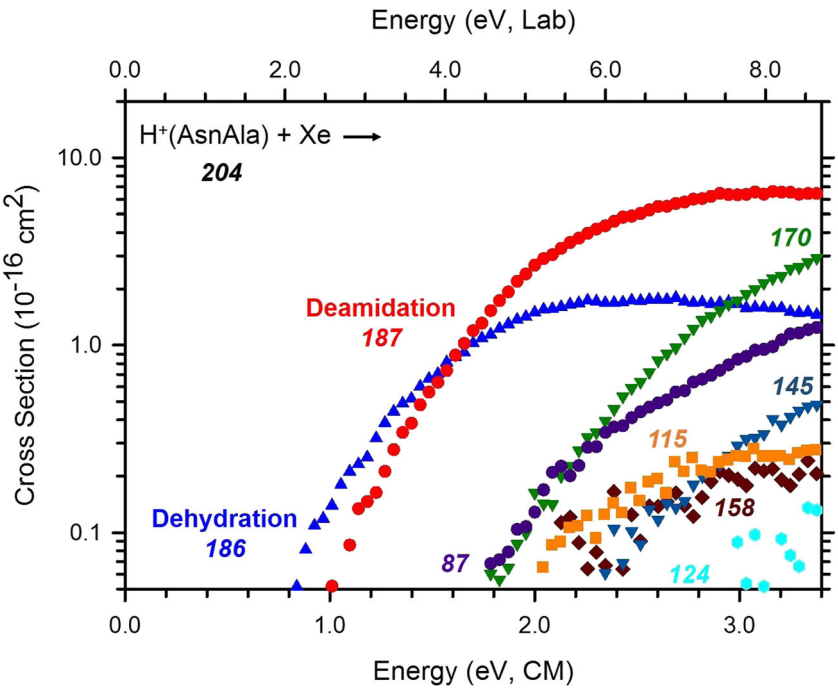

Figure 1. Cross sections for collision-induced dissociation of H^+(AsnAla) with Xe as a function of kinetic energy in the center-of-mass frame (lower *x*-axis) and the laboratory frame (upper *x*-axis). Numbers indicate the mass-to-charge ratio of all ionic species. Cross sections were obtained at a Xe pressure of 0.3 mTorr, under high mass-resolution conditions

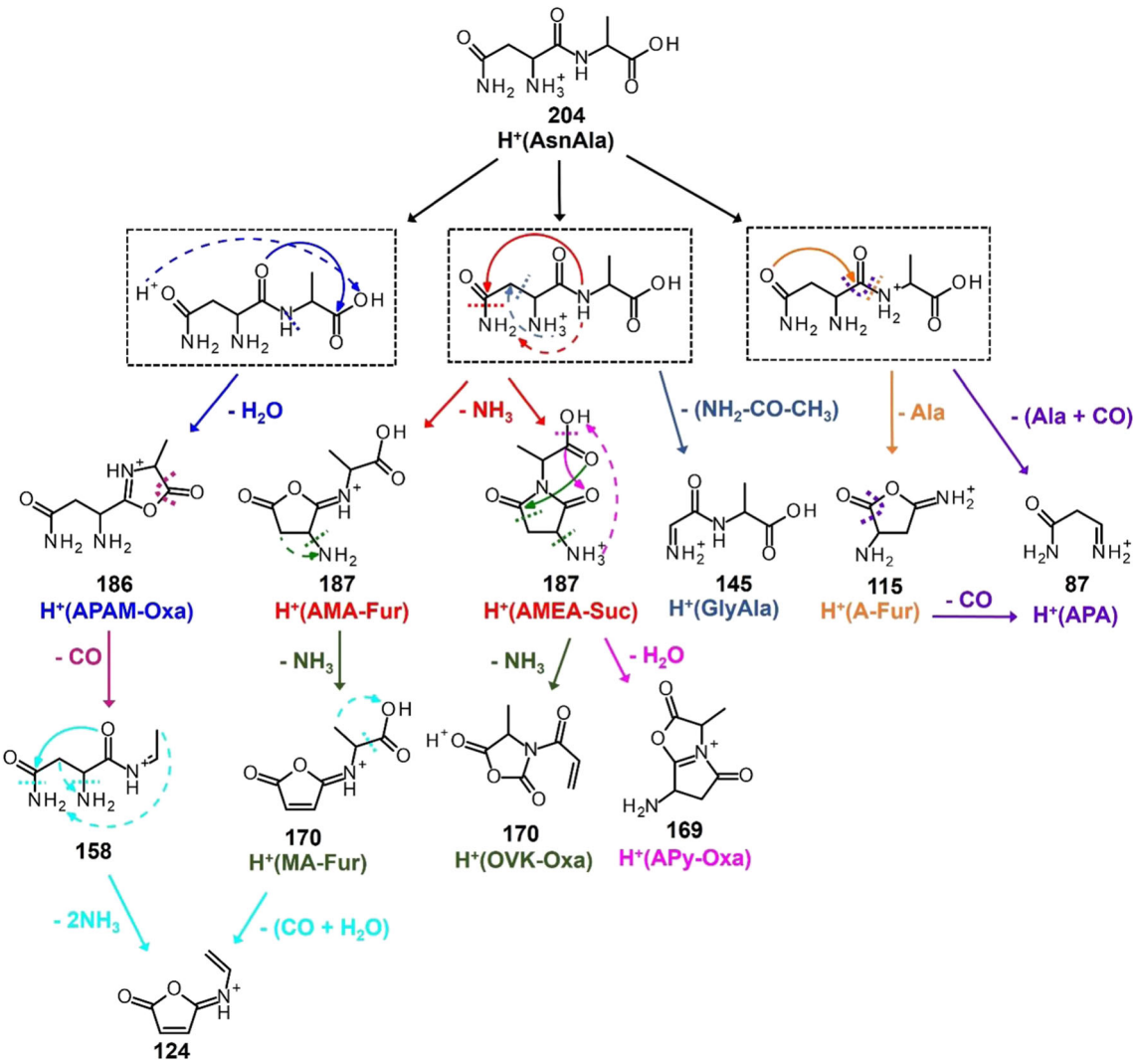

Scheme 2. Major decomposition reaction pathways for H^+(AsnAla) as observed in the TCID and SORI-CID mass spectra. Numbers indicate the mass-to-charge ratio of all ionic species. Dashed lines indicate proton movement; dotted lines indicate bond cleavages; solid lines indicate bond formation. These lines are color-coded to the resulting reaction

threshold and intensity. Likewise, *m/z* 158 and 124 are characterized by high-energy, low-intensity cross sections in both studies. However, the remaining product ions differ in the TCID and SORI-CID studies. These differences can primarily be explained by the slow heating induced by multiple low-energy collisions, which will generally favor the formation of primary ions along the lowest energy pathways. A discussion of how this phenomenon affects the higher energy *m/z* 87, 115, and 145 processes observed only in the TCID studies is given below. Additionally, the Supplementary Material includes an overview of the channel not observed in the high-resolution TCID studies, *m/z* 169.

Theoretical Results for Low-Energy H^+(AsnAla) Conformers

Several low-energy conformations of H^+(AsnAla) were located (Figure 3). Conformers are named according to their protonation sites including additional hydrogen bonds by using the designation [X,Y,Z] where X = protonated atom and Y,Z = site of hydrogen bonds in the order of increasing hydrogen bond length. Backbone nitrogen and oxygen atoms are numbered by residue along the backbone chain starting from the N-terminus. Side-chain nitrogen and oxygen atoms are designated by a superscript s. The protonation site is followed by a series of dihedral angles starting from the N-terminal side-chain amide-group nitrogen to the C-terminal carboxylic acid. Dihedral angles are distinguished as c (cis, for angles between 0° and 45°), g (gauche, 45° and 135°), or t (trans, 135° and 180°).

The four lowest energy conformers are all located within 5 kJ/mol of the GS at all levels of theory and are protonated at the amine nitrogen (N^1) of the backbone. As shown in Figure 3, all four of the N^1 protonation sites interact via hydrogen bonds with the carbonyl oxygen of both the side-chain amide (CO^s) and backbone amide (CO^1), [N^1,CO^s,CO^1]. B3LYP and B3P86 methods predict the [N^1,CO^s,CO^1]-ttgtttt conformer to

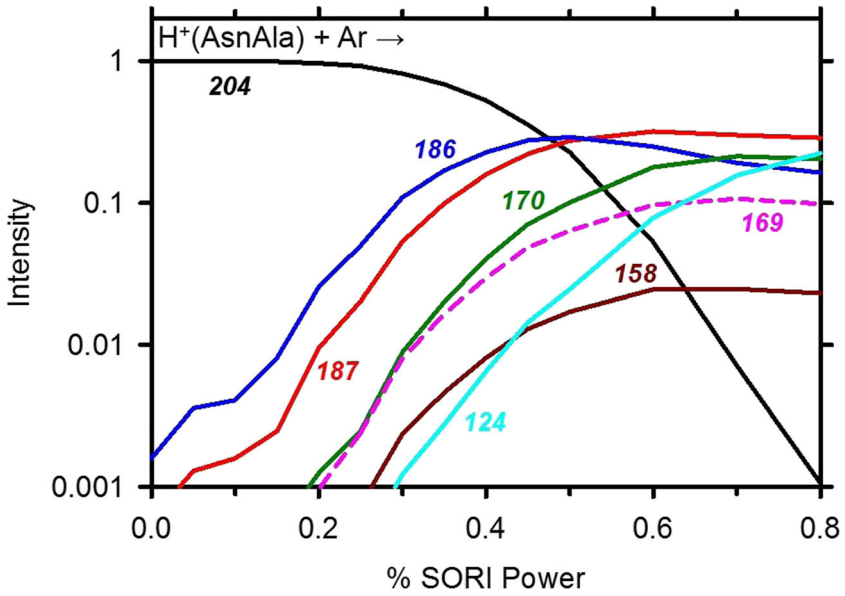

Figure 2. Relative intensities for major SORI-CID fragments of H^+(AsnAla) with Ar as a function of SORI power. Numbers indicate the mass-to-charge ratio of all ionic species. Full lines indicate products that were explicitly observed under high mass-resolution conditions in the TCID studies at all pressures

be lowest in energy, whereas B3LYP-GD3BJ, MP2, and M06-2X predict [N^1,CO^s,CO^1]-gggtgtt to be lowest in energy. These two structures differ in how the carbonyl group of the Ala residue, CO^2, hydrogen bonds: CO^2•HN^2 in ttgtttt and CO^2•HN^s in gggtgtt, a head-to-tail arrangement. Likewise, the ttgtgtt conformer (2–4 kJ/mol above the GS) differs from ttgtttt in that the CO^2•HN^2 hydrogen bond has been lost. Notably, [N^1,CO^s,CO^1]-tgctttt retains the same hydrogen bonding as ttgtttt but at the B3LYP-GD3BJ and M06-2X levels, geometry optimization of this conformer collapses to its GS gggtgtt conformation. An additional 17 conformers having the same protonation site were found 14–40 kJ/mol above the GS (see Figure S1 and Table S1 of the Supplementary Material). Also described in the Supplementary Material are conformers involving alternate protonation sites (see Figure S2, Table S2, and text), as well as mechanisms for moving between select low-energy species. The only alternate protonation site that is relatively low in energy (8–18 kJ/mol above the GS) has the proton on the carbonyl group of the peptide bond, which hydrogen bonds to the side-chain carbonyl, [CO^1,CO^s]. Other alternate protonation sites (Table S2) have energies at least 26 kJ/mol above the GS.

Nomenclature for Major Reaction Species

Nomenclature adopted for each of the key TSs and several of the other major product ions has been described previously [7]. Briefly, cyclic nitrogen and oxygen atoms are designated N^{cx} and O^{cx}, respectively, where *x* indicates the order of appearance. When terminal ends of the dipeptide (carboxylic acid of the deamidation product and side-chain amide of the dehydration product) remain intact, naming is consistent with the nomenclature described above (O^2/O^3 and O^s/N^s, respectively). For TSs where a proton transfer is occurring, protonation sites are designated as [X-Y] where X = protonated atom of the lower energy species and Y = site of transfer. Additional designations are included when additional bonds are being broken {X~Y} or formed {X-Y}.

Theoretical Results for H^+(AsnAla) Deamidation

Under biological conditions, deamidation of asparagine residues is believed to proceed through a cyclic succinimide intermediate. Thus, several TSs for deamidation of H^+(AsnAla) yielding H^+(AMEA-Suc)[N^1,O^2] (shown in Figure 4) were found. An additional pathway that proceeds via a tetrahedral intermediate and leads to a H^+(AMEA-Suc)[O^{c2},O^2] product was also explored, a mechanism that parallels theoretical work by Konuklar et al. on a related neutral peptide model [41]. Notably, Kempkes et al. [11] found that H^+(AsnAla) deamidates to form both the H^+(AMEA-Suc)[N^1,O^2] succinimide (but not the [O^{c2},O^2] isomer) as well as a furanone, H^+(AMA-Fur)[N^2,CO^2,N^1] (Figure 4), such that TSs for formation of this latter product were also explored.

Because the steps leading to rate-limiting TS and product structures are likely to parallel those reported in our H^+(AsnGly) study [7], only key TSs and products are discussed here (see Table 1 and Figure 4). For succinimide formation, the rate-limiting $TS_{N\text{-}Suc}$ leading to H^+(AMEA-Suc)[N^1,O^2] (Figure 4) is 137–163 kJ/mol higher in energy than the GS. Here, $TS_{N\text{-}Suc}$ involves the concerted motions of C-NH_3 bond rupture and ring formation by the amide nitrogen, {H_3N~C,C-N^2}, and is found to be 4–12 kJ/mol higher in energy than the analogous TS found for the decomposition of H^+(AsnGly) [7], a difference attributable to the methyl side chain of Ala. Comparatively, the tetrahedral TS, $TS_{N\text{-}Tet}$, is 65–94 kJ/mol higher in energy than $TS_{N\text{-}Suc}$ and leads to H^+(AMEA-Suc)[O^{c2},O^2], where motions are characterized by concerted proton transfer from O^{c2} to N^s

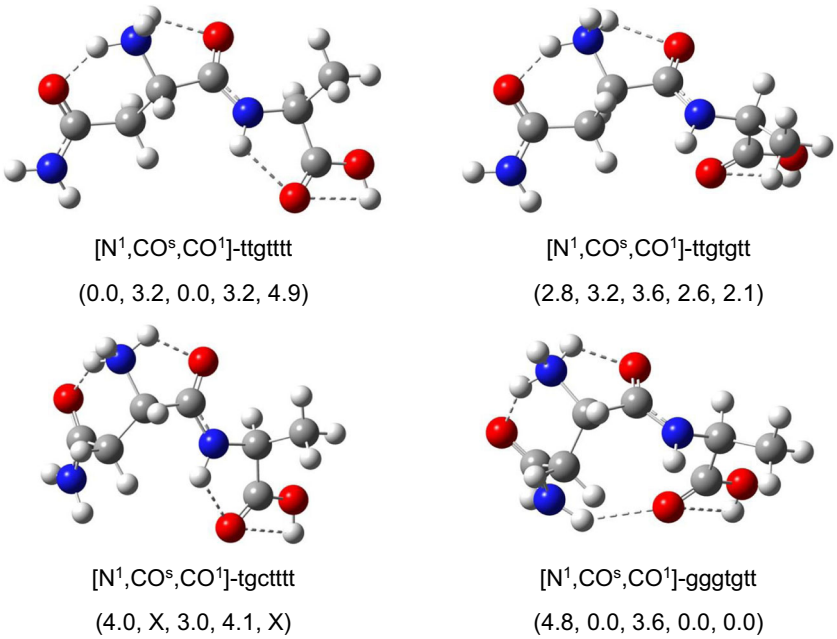

Figure 3. Structures of the four lowest energy H^+(AsnAla) conformers calculated at the B3LYP/6-311+G(d,p) level. Hydrogen bonds are indicated by gray dashed lines. Relative 0 K enthalpies (kJ/mol) are indicated at the B3LYP, B3LYP-GD3BJ, B3P86, MP2, and M06-2X levels of theory, respectively. X indicates the structure collapses to the gggtgtt conformation at that level of theory

and N^1 to O^{c2}. Protonation of AMEA-Suc at $[O^{c2},O^2]$ is 13–33 kJ/mol higher in energy than at $[N^1,O^2]$, Table 1.

Furanone formation via $TS_{N\text{-}Fur}$ also involves concerted C-NH_3 bond rupture and ring formation, but now with the CO^1 carbonyl displacing the ammonia leaving group, $\{H_3N{\sim}C,C\text{-}O^1\}$. $TS_{N\text{-}Fur}$ is lower in energy than $TS_{N\text{-}Suc}$ by 15–32 kJ/mol, Table 1. Interestingly, B3LYP and B3P86 theory predict this process is limited by the tight $TS_{N\text{-}Fur}$ (by 5 and 1 kJ/mol, respectively), whereas the other three levels of theory indicate it is limited by a loose, phase space limit (PSL) TS (by 13 and 5 kJ/mol). In all cases, the furanone rate-limiting step still provides a lower energy barrier for deamidation than succinimide formation by 3–32 kJ/mol. The similar energies of these pathways is consistent with the spectroscopic observation by Kempkes et al. [11] that both H^+(AMEA-Suc) and H^+(AMA-Fur) products are formed experimentally. This prediction is particularly important as the presence of both furanone and succinimide complexes at higher energies may affect the sequential channels observed, as discussed in more detail in the following sections.

Theoretical Results for H^+(AsnAla) Dehydration

At all levels of theory, the lowest energy pathway located for dehydration of H^+(AsnAla) is shown to proceed through tight TS_O (97–122 kJ/mol higher in energy than the GS) (Table 1 and Figure 5). Here, TS_O is characterized by motions of a proton transfer from CO^s to O^3H, bond rupture of $C{\sim}O^3$, and ring formation ($C\text{-}O^1$). Similar to that found in our H^+(AsnGly) study [7], this TS leads to an oxazolone product, H^+(APAM-Oxa)$[N^2,N^1]$, which is 8–24 kJ/mol lower in energy than TS_O and 90–105 kJ/mol higher than the GS. Dehydration is favored by 33–44 and 13–37 kJ/mol, when compared to the rate-limiting TSs for succinimide and furanone formation, respectively.

Theoretical Results for the Formation of m/z 87 from H^+(AsnAla)

The lowest energy pathway leading to formation of *m/z* 87 parallels that reported for the analogous process in the decomposition of H^+(AsnGly) [7]. Here, TS_A (165–196 kJ/mol higher in energy than the GS) involves the concerted motions of $C{\sim}CO^1$ and $O^1C{\sim}N^2$ bond ruptures (Figure 5). This TS is predicted to be rate-limiting at the B3LYP level of theory, 11 kJ/mol above the final products, H^+(APA)$[N^1,CO^s]$ + CO + Ala. The remaining levels of theory predict a loose, PSL TS at the product asymptote, which lies higher in energy than TS_A by 8–26 kJ/mol. An additional pathway involving sequential formation of *m/z* 87 from the primary product *m/z* = 115 is detailed in the Supplementary Material text and Figure S3. Table 1 indicates that the energies for this process are limited by TS_{SA}, 230–267 kJ/mol above the GS.

Theoretical Results for the Formation of m/z 170 and 169 from m/z 187, and m/z 169 from m/z 186

Our theoretical results suggest that both *m/z* 170 and 169 can be formed sequentially from *m/z* 187 by ammonia and water losses, respectively. The lowest energy pathway for secondary ammonia loss proceeds via a tight $TS_{SN\text{-}MA\text{-}Fur}$ (Figure 6) located 306–340 kJ/mol higher in energy than the GS and 24–54 kJ/mol lower in energy than sequential ammonia loss from H^+(AMEA-Suc) via $TS_{SN\text{-}OVK\text{-}Oxa}$ (Table 1). Here, $TS_{SN\text{-}MA\text{-}Fur}$ involves hydrogen atom transfer from a carbon to

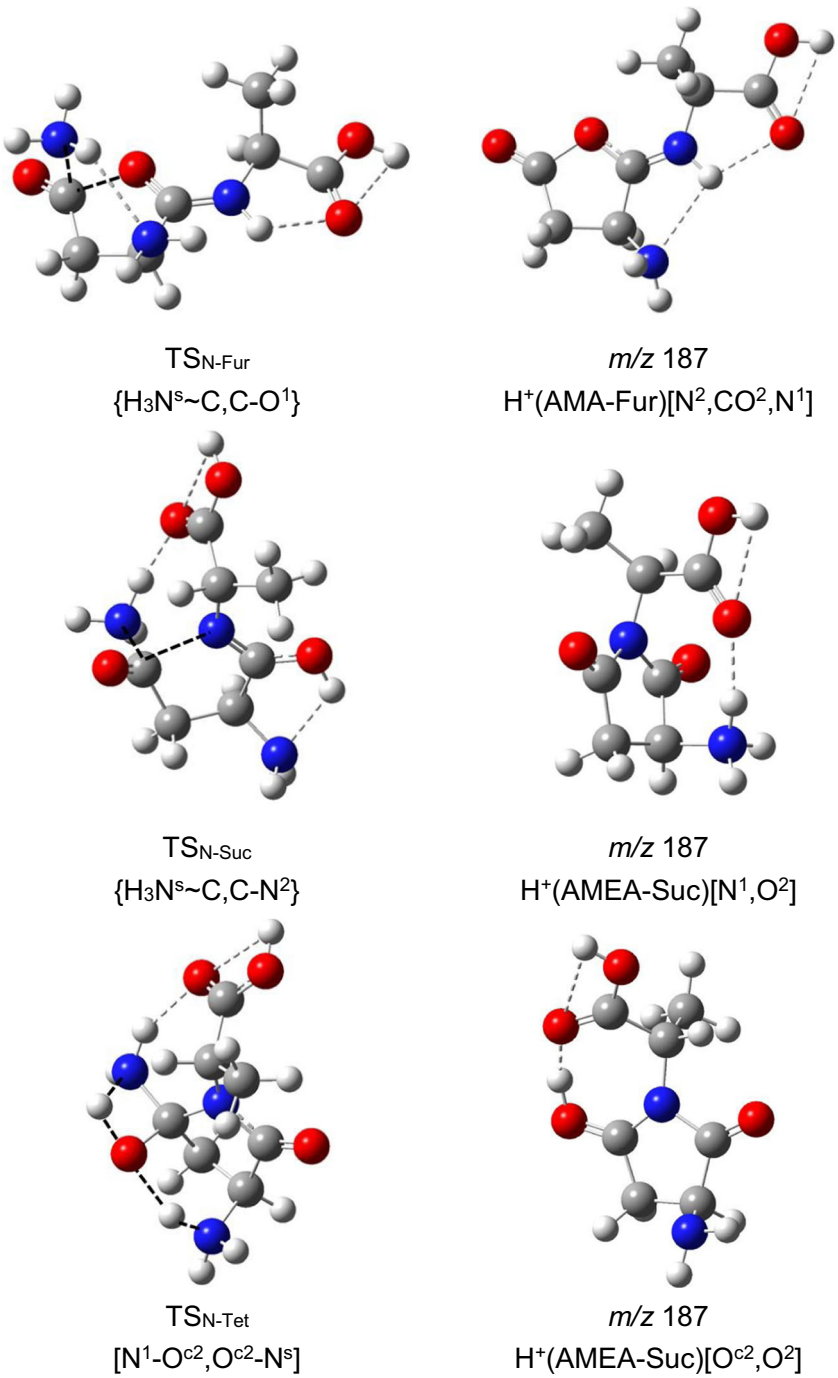

Figure 4. Rate-limiting TSs and product structures of deamidation reactions calculated at the B3LYP/6-311+G(d,p) level. Hydrogen bonds are indicated by gray dashed lines. Bond rupture and formation are designated by black dashed lines

the N-terminus, which is followed at lower energies by loss of the newly formed NH_3 (C~N^1) and ring closure (C-O^1) to reform the furanone ring.

The lowest energy pathway forming *m/z* 169 results from loss of water from H$^+$(AMEA-Suc) via TS$_{SO\text{-}Py\text{-}Oxa}$ (Figure 6). In this TS, loss of water is aided by ring closure to form the bicyclic H$^+$(APy-Oxa)[N^c] product. B3LYP and B3P86 predict this tight TS is rate-limiting (but only by 2–3 kJ/mol), whereas B3LYP, MP2, and M06-2X levels of theory indicate the loose PSL TS at the product asymptote is rate-limiting (by 20–33 kJ/mol). Loss of water from the succinimide product ion is lower than the analogous loss of ammonia by 113–152 kJ/mol. This is consistent with the observation by Kempkes et al. that the succinimide product undergoes further decomposition by water loss to form H$^+$(Apy-Oxa)[N^c], whereas the furanone product undergoes sequential ammonia loss to form H$^+$(MA-Fur)[N^2]. In both cases, the products were identified spectroscopically [11]. Additional higher energy pathways leading to *m/z* 169 are detailed in the Supplementary Material text and Figure S4.

Table 1. Relative 0 K Enthalpies of Key Reaction Species for the Decomposition of H^+(AsnAla)

Ionic product	Neutral product	TS	B3LYP	B3LYP-GD3BJ[a]	B3P86	MP2	M06-2X[b]
m/z 186	H_2O	TS_O	*119.1*	*110.3*	*121.6*	*97.5*	*115.5*
H^+(APAM-Oxa) [N^2,N^1]		PSL	95.0	105.4	101.2	89.6	103.6
m/z 187	NH_3	$TS_{N\text{-}Fur}$	*131.8*	131.4	*138.5*	121.2	137.6
H^+(AMA-Fur) [N^2,CO^2,N^1]		PSL	126.3	*144.5*	137.4	*134.1*	*142.1*
m/z 170	2 NH_3	$TS_{SN\text{-}MA\text{-}Fur}$	*306.2*	*322.0*	*319.5*	*314.0*	*339.6*
H^+(MA-Fur)[N^2]		PSL	176.7	209.8	209.2	206.6	225.6
m/z 187	NH_3	$TS_{N\text{-}Suc}$	163.3	153.9	154.8	136.8	152.1
H^+(AMEA-Suc) [N^1,O^2]		PSL	103.9	105.2	107.5	82.2	104.5
m/z 187	NH_3	$TS_{N\text{-}Tet}$	256.9	240.7	229.0	202.1	225.1
H^+(AMEA-Suc) [O^{c2},O^2]		PSL	117.5	126.9	120.9	115.1	123.7
m/z 170	2 NH_3	$TS_{SN\text{-}OVK\text{-}Oxa}$	333.7	346.0	373.6	338.0	379.9
H^+(OVK-Oxa)[O^3]		PSL	289.0	315.4	325.6	315.0	333.6
m/z 169	$NH_3 + H_2O$	$TS_{SO\text{-}Py\text{-}Oxa}$	*221.3*	221.9	*237.0*	185.9	231.5
H^+(APy-Oxa)[N^c]		PSL	219.5	*243.3*	234.0	*218.8*	*251.2*
m/z 115	Ala	$TS_{A\text{-}AF}$	136.8	138.1	147.6	132.4	139.5
H^+(A-Fur)[N^s]		PSL	*178.4*	*204.8*	*192.3*	*204.7*	*201.6*
m/z 87	Ala + CO	TS_{SA}	230.3	256.6	266.7	265.9	267.2
H^+(APA)[N^1,CO^s]		PSL	153.8	192.5	204.1	188.7	193.2
m/z 87	Ala + CO	TS_A	*165.1*	166.7	196.0	180.7	174.6
H^+(APA)[N^1,CO^s]		PSL	153.8	*192.5*	*204.1*	*188.7*	*193.2*

Relative 0 K single point enthalpies calculated at the level of theory indicated using a 6-311+G(2d,2p) basis set and B3LYP/6-311+G(d,p) geometries. Italic values indicate the rate-limiting energy for each reaction

[a]Calculated at the B3LYP-GD3BJ/6-311+G(2d,2p)//B3LYP-GD3BJ/6-311+G(d,p) level of theory

[b]Calculated at the M06-2X/6-311+G(2d,2p)//M06-2X/6-311+G(d,p) level of theory

Cross-Section Modeling

Equation 1 was used to analyze the cross sections for the primary deamidation, dehydration, and concomitant Ala and CO loss decomposition channels of H^+(AsnAla). Simultaneous modeling of these primary channels using Eq. 1 accounts directly for competition among these channels. Several approaches to modeling the data were used, as detailed in the Supplementary Material text. Final data analysis involved utilizing a switching TS model for the deamidation reaction and formation of *m/z* 87 because theory suggests that both tight and loose parameters could be controlling these decomposition channels, whereas dehydration was modeled using parameters for the tight TS_O. This switching TS analysis has been described elsewhere [7] and details can be found in the Supplementary Material. In general, final data analysis involved an approach where self-consistent threshold energies were obtained for the tight and PSL TSs. For both deamidation and concomitant loss of Ala and CO, the PSL threshold energies are upper limits, such that they are fully consistent with any theoretical predictions that lie at lower energies. We also found that the low-frequency modes of TS_O needed to be tightened (increased) by ~15% in order to obtain an appropriate fit in the threshold region, while leaving the frequencies for $TS_{N\text{-}Fur}$ intact. Likewise, low-frequency modes of TS_A leading to formation of *m/z* 87 needed to be tightened by 5%. The *m/z* 170 sequential channel was analyzed using parameters for tight $TS_{SN\text{-}MA\text{-}Fur}$, which proceeds via the H^+(AMA-Fur) primary ion. In order to reproduce this channel in the threshold region, low-frequency modes of this TS were loosened (decreased) by ~50%, similar to the magnitude used previously in the analogous sequential decomposition of H^+(AsnGly) [7]. The scaling of low-frequency modes (< 900 cm^{-1}) in several channels was needed to properly model the competitive dissociation behavior, but this is consistent with Gaussian warnings that such frequencies are not always reliable [35]. Using the parameters given in Table 2, the data were reproduced over the full energy and magnitude ranges with Figure 7 showing one example. (The data in Figure 7 differ from that in Figure 1 in that they correspond to extrapolation of the cross sections to zero pressure, rigorously single collision conditions.)

As detailed in the Supplementary Material, we also considered the possibility that formation of both H^+(AMEA-Suc) and H^+(AMA-Fur) could contribute to the observed cross section for formation of *m/z* 187 (Figure S5). From such an analysis, we conclude that formation of the succinimide could contribute to the observed cross section at energies beginning about 0.14 eV (14 kJ/mol) above the threshold determined for furanone formation. This energy difference agrees nicely with theory, which predicts a difference in the two pathways ranging from 3 to 32 kJ/mol (and an average of 18 ± 11 kJ/mol). Notably, if the cross section is modeled using only tight $TS_{N\text{-}Suc}$ parameters, the threshold does not agree well with theory, as discussed further below.

As noted above, thresholds were also determined without including RRKM modeling and competition in order to estimate kinetic and competitive shifts (Table 2). These shifts are sufficiently large that the good agreement between experiment and theory discussed below would *not* be obtained without including these effects. Average kinetic shifts for tight and PSL TSs are 0.92 and 0.59 eV, respectively, such that the relative magnitudes of these values are consistent with the tight and loose character of these pathways [42]. This character is also fairly well-described by the entropies of activation

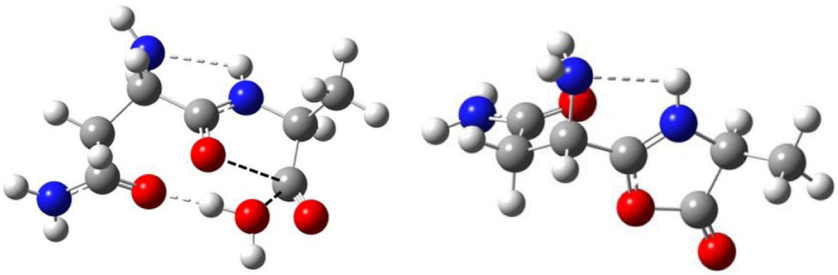

TS_O — *m/z* 186

$\{O^3\sim C, C\text{-}O^1\}$ — $H^+(APAM\text{-}Oxa)[N^2, N^1]$

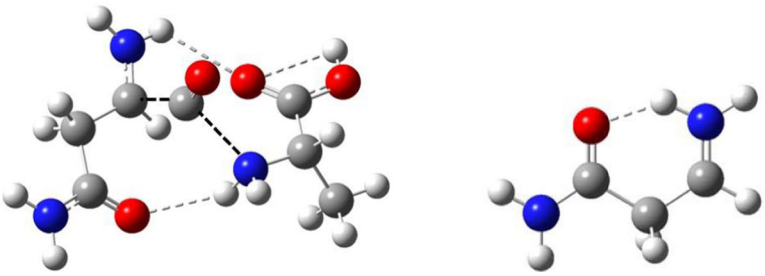

TS_A — *m/z* 87

$\{C\sim CO^1, O^1C\sim N^2\}$ — $H^+(APA)[N^1, CO^s]$

Figure 5. Rate-limiting TSs and product structures of dehydration and *m/z* 87 reactions calculated at the B3LYP/6-311+G(d,p) level. Hydrogen bonds are indicated by gray dashed lines. Bond rupture and formation are designated by black dashed lines

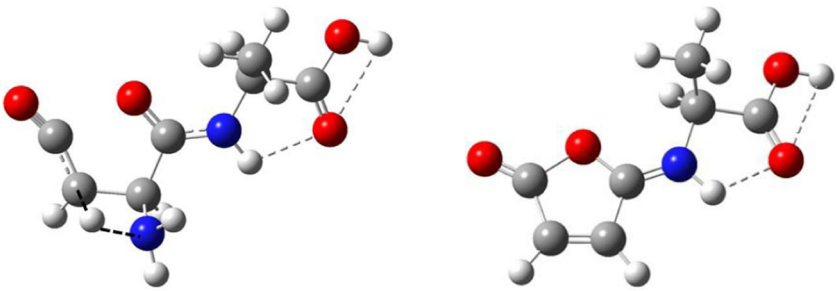

$TS_{SN\text{-}MA\text{-}Fur}$ — *m/z* 170

$[C\text{-}N^1]$ — $H^+(MA\text{-}Fur)[N^2]$

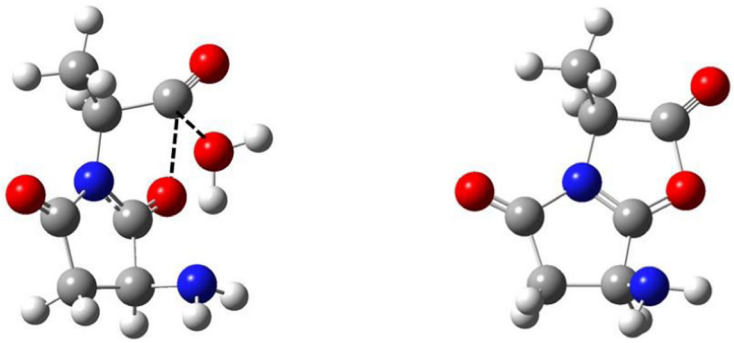

$TS_{SO\text{-}Py\text{-}Oxa}$ — *m/z* 169

$\{H_2O^3\sim C, C\text{-}O^{c2}\}$ — $H^+(APy\text{-}Oxa)[N^c]$

Figure 6. Rate-limiting TSs and product structures leading to the formation of *m/z* 170 and 169 calculated at the B3LYP/6-311+G(d,p) level. Hydrogen bonds are indicated by gray dashed lines. Bond rupture and formation is designated by black dashed lines

Table 2. Fitting Parameters of Eq. 1, Threshold Energies at 0 K, and Entropies of Activation at 1000 K for Cross Sections of the Reactions Indicated

Ionic product	Neutral product	TS	Frequency scaling[a]	σ_0	n	E_0 (eV)	E_0 (eV) (no RRKM)	$\Delta S^{\dagger}_{1000}$ (J/K mol)
m/z 186	H_2O	TS_O	1.15	14.0 (2.5)	1.3 (0.2)	1.07 (0.07)	1.80 (0.12)	−61 (2)[b]
m/z 187	NH_3	$TS_{N\text{-}Fur}$	1.00	″	″	1.28 (0.05)	2.27 (0.11)	−3 (0.4)
m/z 187	NH_3	PSL_{Fur}	1.00	″	″	< 1.64 (0.08)	2.27 (0.11)	59 (3)
m/z 87	Ala + CO	TS_A	1.05	″	″	1.61 (0.08)	2.94 (0.12)	35 (8)[c]
m/z 87	Ala + CO	PSL_A	1.05	″	″	< 2.39 (0.16)	2.94 (0.12)	201 (7)[d]
m/z 170	2 NH_3	$TS_{SN\text{-}MA\text{-}Fur}$	0.50	″	″	3.02 (0.07)	3.63 (0.28)	98 (8)[e]

Uncertainties (one standard deviation) in parentheses
[a]Scaling factor applied to frequencies < 900 cm^{-1}
[b]$\Delta S^{\dagger}_{1000}$ determined without frequency scaling is −30 (1) J/K mol
[c]$\Delta S^{\dagger}_{1000}$ determined without frequency scaling is 42 (0.4) J/K mol
[d]$\Delta S^{\dagger}_{1000}$ determined without frequency scaling is 206 (4) J/K mol
[e]$\Delta S^{\dagger}_{1000}$ determined without frequency scaling is −66 (7) J/K mol

determined for the rate-limiting TSs. Notably, both deamidation and dehydration are limited by tight TSs such that negative entropies of activation result, −3 and −61 J/K mol, respectively. On this basis, dehydration is less entropically favorable than deamidation, which explains its smaller cross section even though it is enthalpically favored.

Conversion of Thermodynamic Parameters from 0 to 298 K

For comparison of the thermodynamic information obtained here experimentally to room temperature conditions, Table 3 provides the conversion from 0 K thresholds to 298 K enthalpies and Gibbs energies. This conversion was accomplished using the rigid rotor/harmonic oscillator approximations with rotational constants and vibrational frequencies calculated at the B3LYP/6-311+G(d,p) level. Uncertainties listed were determined by scaling the vibrational frequencies by ± 10%.

Discussion

TCID Versus SORI-CID

Comparison of the TCID cross sections (Figure 1) with the SORI-CID results (Figure 2) show fairly similar cross-section behavior for the main channels of interest, namely the deamidation and dehydration channels. In the TCID and SORI studies, dehydration appears at lower threshold energies and

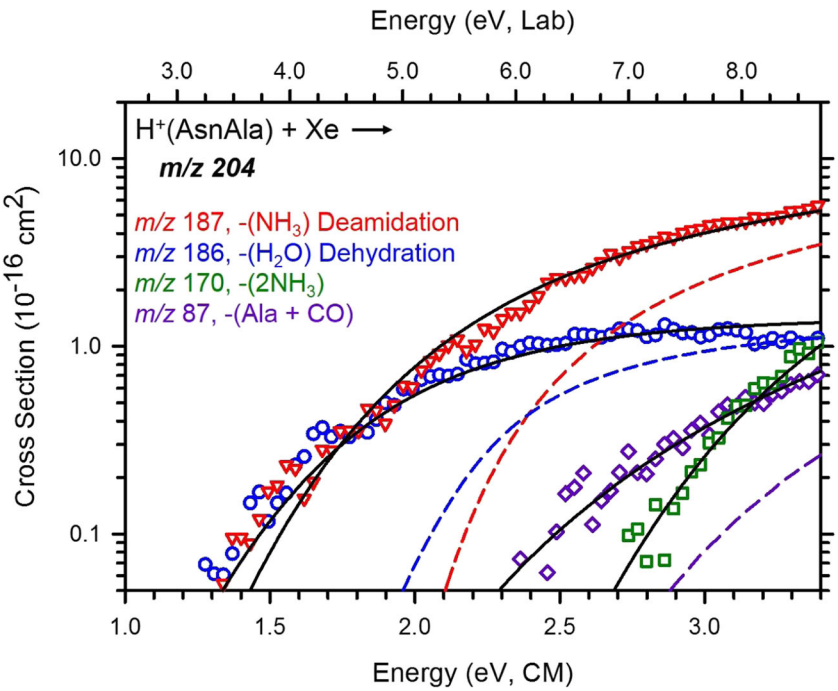

Figure 7. Cross-section models of the main decomposition products of H^+(AsnAla) as a function of collision energy with Xe in the center-of-mass frame (lower *x*-axis) and the laboratory frame (upper *x*-axis). Solid lines show the best fit to the zero-pressure extrapolated data (open symbols) using the model of Eq. 1 convoluted over the neutral and ion kinetic and internal energy distributions. Dashed lines show the model cross sections in the absence of experimental kinetic energy broadening for reactants with an internal energy of 0 K

Table 3. Enthalpies and Gibbs Energies of Reaction at 0 and 298 K for Decomposition Reactions of H^+(AsnAla)

Ionic product	Neutral product	TS	ΔH_0[a]	ΔH_{298}-ΔH_0[b]	ΔH_{298}	$T\Delta S_{298}$[b]	ΔG_{298}
m/z 186	H_2O	TS_O	103 (6)	1.2 (0.2)	104 (6)	− 9.3 (0.1)	114 (6)
				− 1.7 (0.1)	*101 (7)*	*− 15.4 (0.5)*	*117 (5)*
m/z 187	NH_3	$TS_{N\text{-}Fur}$	123 (5)	3.6 (0.1)	127 (4)	− 1.2 (0.2)	128 (4)
m/z 187	NH_3	PSL_{Fur}	< 159 (8)	4.5 (0.3)	163 (8)	45.9 (0.9)	117 (8)
m/z 87	Ala + CO	TS_A	155 (7)	6.8 (0.1)	162 (7)	9.9 (0.5)	152 (7)
				6.2 (0.7)	*161 (7)*	*8.4 (1.7)*	*153 (7)*
m/z 87	Ala + CO	PSL_A	< 230 (16)	9.3 (0.5)	240 (16)	85.5 (0.5)	154 (15)
				8.8 (0.7)	*239 (16)*	*84.3 (1.5)*	*155 (15)*
m/z 170	2 NH_3	$TS_{SN\text{-}MA\text{-}Fur}$	291 (6)	− 0.4 (1.0)	290 (6)	0.9 (0.8)	289 (6)
				13.5 (0.7)	*305 (6)*	*38.0 (1.9)*	*267 (7)*

Uncertainties in parentheses
[a]Experimental values from Table 2
[b]Calculated using standard formulas and molecular constants calculated at the B3LYP/6-311+G(d,p) level. Uncertainties are calculated from variations of ± 10% in the vibrational frequencies. Values in italics utilize the scaled frequencies used to reproduce the magnitude of the data (see text and Table 2)

powers, respectively, where the competitive deamidation channel becomes dominant at around 1.6 eV and 0.5% SORI power, respectively. Here, characterization of similar cross-section behavior in both studies indicates that although the collisional aspects of these two techniques are distinctly different, qualitative behavior can translate between the two. Furthermore, these similarities show that the mass-resolution conditions used in the TCID study were sufficient to accurately distinguish these channels (separated by only 1 amu) without sacrificing efficient transmission. Similar behavior was also observed for the sequential *m/z* 170 channel, where in both TCID and SORI studies, *m/z* 170 appears at higher energies than both deamidation and dehydration, consistent with its sequential behavior. Further, its magnitude is larger than that for dehydration, although smaller than that for deamidation at the highest energies and powers used. Similarly, the energy dependence of the *m/z* 158 and 124 channels observed in the TCID cross sections parallels that observed in the SORI study in their respective threshold regions.

Differences between the TCID and SORI-CID results arise primarily because of product channels observed in one study and not the other. Three additional channels (*m/z* 87, 115, and 145) not observed in the SORI analysis were measured in the TCID studies. Here, *m/z* 145 and *m/z* 115 are both characterized as high-energy primary channels (Scheme 2). High-energy primary ions observed in TCID studies are generally a result of being entropically favored once enough energy is available, whereas the multiple, slow-heating collisions of SORI favor low-energy products (deamidation and dehydration) such that these higher energy *m/z* 145 and 115 primary channels are not observed. The slow-heating phenomenon also explains why the lower energy dehydration channel has relatively larger intensity than the deamidation channel in the SORI-CID results compared to the TCID results. Similar findings were also observed in the H^+(AsnGly) study [7], although there, *m/z* 87 was observed in both TCID and SORI-CID studies. The failure to observe this species in the current SORI-CID study does not have a particularly clear explanation, given that the measured threshold for this channel is slightly lower in energy than observed previously for the analogous loss in the H^+(AsnGly) study [7].

The only channel observed in the SORI study but not by TCID is *m/z* 169, which is formed in a sequential process by water loss from the primary H^+(AMEA-Suc) product, as detailed in the Supplementary Material. The failure to observe this product in the high mass-resolution TCID work can probably be attributed to its small intensity (as observed in the SORI studies at low SORI powers and the cross sections measured under low mass-resolution conditions, see Figure S6 and Supplementary Material text) and proximity to the more abundant *m/z* 170 product.

Experimental Versus Theoretical Results

Our best values for the experimental threshold energies come from the analysis in which all three primary channels are simultaneously modeled and switching transition states are considered for both deamidation and formation of *m/z* 87. Other simpler approaches (detailed in Table S3) provide threshold energies that are very similar. These experimental values are compared with calculated quantum chemical 0 K reaction energies in Table 4. For the deamidation process leading to furanone formation, the experimentally determined thresholds (via its tight and PSL TSs) were found to be 123 ± 5 kJ/mol and < 159 ± 8 kJ/mol, respectively. The tight TS threshold determined is within experimental uncertainty of the predicted $TS_{N\text{-}Fur}$ energy at the MP2 (121 kJ/mol) level of theory, and within two standard deviations at the B3LYP and B3LYP-GD3BJ levels. The remaining levels of theory predict reaction energies ~3 standard deviations higher in energy, where B3P86 predicts the highest $TS_{N\text{-}Fur}$ energy of 139 kJ/mol. The upper limit to the threshold found using PSL TS parameters is 14–33 ± 8 kJ/mol greater than the predicted reaction energies at all levels of theory. Thus, we conclude that the tight $TS_{N\text{-}Fur}$ is the rate-limiting TS even if the product asymptote lies at slightly higher energies, as confirmed by the switching TS analysis. Notably, modeling this deamidation channel using succinimide formation parameters alone ($TS_{N\text{-}Suc}$) results in a threshold of 112 ± 6 kJ/mol (Table S3), 25–51 kJ/mol *lower* than predicted reaction energies at all levels of theory. Thus,

Table 4. Experimental and Theoretical Reaction Energies at 0 K (kJ/mol) for Decomposition Reactions of H^+(AsnAla)

Ionic product	Neutral product	TS	Exp[a]	B3LYP[b]	B3LYP-GD3BJ[c]	B3P86[b]	MP2[b]	M06-2X[d]
m/z 186	H_2O	TS_O	103 (6)	119	110	122	98	116
m/z 187	NH_3	$TS_{N\text{-}Fur}$	123 (5)	132	131	139	121	138
m/z 187	NH_3	PSL_{Fur}	< 159 (8)	126	145	137	134	142
m/z 87	Ala + CO	TS_A	155 (7)	165	167	196	181	175
m/z 87	Ala + CO	PSL_A	< 230 (16)	154	193	204	189	193
m/z 170	2 NH_3	$TS_{SN\text{-}MA\text{-}Fur}$	291 (6)	306	322	320	314	340
MADs [e]				13 (4)	15 (13)	26 (11)	14 (12)	25 (19)

[a]Experimental values from Table 3. Uncertainties in parentheses
[b]Calculations performed at the stated level of theory using a 6-311+G(2d,2p) basis set with geometries calculated at B3LYP/6-311+G(d,p) level, ZPE corrections included
[c]Calculations performed at B3LYP-GD3BJ/6-311+G(2d,2p)//B3LYP-GD3BJ/6-311+G (d,p) level, ZPE corrections included
[d]Calculations performed at the M06-2X/6-311+G(2d,2p)//M06-2X/6-311+G(d,p) level, ZPE corrections included
[e]Calculated mean absolute deviations (MADs) from four experimental values obtained using tight TS parameters for *m/z* 187 and 87 in the switching TS analysis

the deamidation threshold can be assigned unambiguously to furanone formation, although succinimide formation can contribute at higher energies.

Competitive analysis of the dehydration channel determined that the experimental threshold is 103 ± 6 kJ/mol, nearly within experimental uncertainty of the B3LYP-GD3BJ (110 kJ/mol) and MP2 (98 kJ/mol) reaction energies. All remaining levels of theory predict energies greater than two standard deviations higher than our measured threshold. Similar to the deamidation energies, B3P86 provides the highest reaction barrier (122 kJ/mol). One can also consider the relative differences between experimental thresholds (found using tight TS parameters) of the two channels, 20 ± 5 kJ/mol. B3P86, B3LYP-GD3BJ, M06-2X, and MP2 predict this difference well, 17, 21, 22, and 23 kJ/mol, respectively, whereas B3LYP is lower, 13 kJ/mol.

Similar agreement is observed between experiment and theory for the primary Ala and CO loss and secondary ammonia loss channels. Here, the switching TS analysis for *m/z* 87 using tight TS parameters resulted in a threshold value of 155 ± 7 kJ/mol, nearly within experimental uncertainty of the B3LYP predicted reaction energy of 165 kJ/mol. Notably, this level of theory is the only level that predicted a tight TS-limited reaction. The experimentally determined upper limit for the PSL asymptote was determined to be < 230 ± 16 kJ/mol, in agreement with all calculations, which are lower by 26–76 ± 16 kJ/mol. These results again indicate that the tight TS is playing a significant role in controlling the rate of reaction, even at the product asymptotic energies. For the sequential *m/z* 170 channel (loss of 2 NH_3), the B3LYP predicted reaction energy of 306 kJ/mol lies just outside two standard deviations of the measured threshold, 291 ± 6 kJ/mol, with other levels of theory somewhat higher.

Also shown in Table 4 are calculated mean absolute deviations (MADs) between experiment and all five levels of theory. MADs were calculated using only the tight TS energies for the channels analyzed using the switching TS method (as our switching analysis confirmed that these tight TSs appear to control the rate of reaction, such that the PSL thresholds are truly upper limits). The lowest MADs were observed for B3LYP, B3LYP-GD3BJ, and MP2 levels of theory, ~14 kJ/mol. Not including the sequential channel decreases the MADs by 1–6 kJ/mol for these three levels of theory. Notably, MADs calculated for B3P86 and M06-2X were characteristically much higher. The consistent agreement between theory and experiment for these modeled channels at the B3LYP, B3LYP-GD3BJ, and MP2 levels of theory suggests that the necessary experimental conditions to produce thermal ions were used and confirms that the mechanisms located for these reactions are reasonable pathways.

C-Terminal Residue Side-Chain Effects

As presented here, the comparative analysis of key theoretical and experimental findings between the current and H^+(AsnGly) [7] studies allows for the determination of the adjacent C-terminal residue side-chain effects, i.e., H versus CH_3. Experimentally, cross-section behavior for the key reactions of interest are similar in both H^+(AsnGly) [7] and H^+(AsnAla) studies. Competitively, the dehydration channel appears at slightly lower energies than deamidation, by 12 kJ/mol for H^+(AsnGly) and by 20 kJ/mol for H^+(AsnAla). In both cases, dehydration exhibits a much lower intensity, a consequence of a tighter rate-limiting TS, such that the dominant channel is deamidation at all energies except near the observed thresholds. However, in our previous H^+(AsnGly) study [7], furanone formation likely dominated the deamidation channel at elevated energies (as confirmed by modeling the experimental data using molecular parameters from both pathways), although modeling of the threshold region suggested that succinimide formation was favored at threshold energies. The current analysis indicates that the opposite behavior occurs for H^+(AsnAla), where both energetics and cross-section modeling suggest that furanone formation is favored at threshold energies with the succinimide contributing at higher energies. Interestingly, we observe more dissociation channels in the current H^+(AsnAla) study (under high-resolution conditions) such that two additional primary channels are also measured, although these channels are high in energy and characterized by a low intensity. The observance of these channels in the current study may simply be a result of a greater intensity of the precursor

H^+(AsnAla) ion beam when compared to that obtained in the previous H^+(AsnGly) study, potentially a side effect of the faster deamidation rates of AsnGly sequences [4].

This observation of relative stabilities conceivably suggests that deamidation of AsnGly sequences could exhibit measurably lower thresholds for deamidation than AsnAla sequences in particular. Indeed, for succinimide formation, the rate-limiting $TS_{N\text{-}Suc}$ calculated here is higher in energy than the analogous TS in the H^+(AsnGly) study at all levels of theory (by 4–12 kJ/mol) [7], consistent with the faster deamidation rates observed with AsnGly sequences in solution [4]. Thus, the addition of the methyl side chain in Ala does appear to have an energetic effect on the deamidation pathway yielding the succinimide product. However, the methyl side chain also influences the dynamics of the reaction in the gas-phase such that furanone (rather than succinimide) formation is preferred in the current case. This leads to very similar theoretical reaction energies being obtained for the deamidation channel when considering the lowest energy pathways found for H^+(AsnGly) versus H^+(AsnAla). In the current analysis, H^+(AMA-Fur) formation via $TS_{N\text{-}Fur}$ (132 and 139 kJ/mol relative to the GS at the B3LYP and B3P86 levels, which predict a tight TS-limited reaction) is only 0.5 and 0.8 kJ/mol lower in energy, respectively, than the analogous pathway found in the H^+(AsnGly) study. Similarly, the product asymptote of H^+(AMA-Fur) + NH_3 is nearly isoenergetic with that of the furanone products in the H^+(AsnGly) study (difference of 3–6 kJ/mol at the B3LYP-GD3BJ, MP2, and M06-2X levels of theory, which predict a loose PSL-limited TS).

From a structural point of view, the energetic cost associated with the methyl group appears to be related to its proximity to key molecular vibrations in the rate-limiting TSs. For succinimide formation, $TS_{N\text{-}Suc}$ ring formation occurs at the nitrogen adjacent to the methyl substitution site (Figure 4), such that steric and energetic effects are more pronounced when Ala is present. In contrast, furanone formation involves ring formation much closer to the N-terminus, with no indication of being sterically affected by the methyl group, as indicated by very similar reaction energies predicted in the AsnGly and AsnAla systems.

It is also valuable to consider the experimental thresholds measured for the lowest energy pathway for deamidation from H^+(AsnGly) and H^+(AsnAla). Succinimide formation from H^+(AsnGly) resulted in a measured threshold of 129 ± 6 kJ/mol [7]. Comparatively, furanone formation from H^+(AsnAla) (theoretically predicted to be lower in energy than succinimide formation) was measured to have a slightly lower threshold of 123 ± 5 kJ/mol. Thus, although theoretical reaction energies suggest there should be an increasing energetic trend for deamidation via succinimide formation, these gas-phase dipeptide systems clearly have alternative decomposition pathways (here, furanone formation) characterized by similar reaction barriers. Notably, the cross-section analysis of the deamidation channels is somewhat distinct in the H^+(AsnGly) and H^+(AsnAla) studies. Deamidation of H^+(AsnGly) via succinimide formation is controlled by a tight TS, as is furanone formation in the current study. In both cases, low-frequency modes of the competitive dehydration channel were scaled in order to best fit the deamidation cross section, by 20% in the H^+(AsnGly) study [7] and by 15% for H^+(AsnAla).

Predicted reaction energetics appear to show an enhancement for the dehydration pathway from H^+(AsnAla) compared to H^+(AsnGly). Here, theoretical energies for TS_O are 7–13 kJ/mol lower in energy than those calculated for H^+(AsnGly) [7]. Experimental thresholds exhibit similar behavior, where the threshold for dehydration of H^+(AsnAla) (103 ± 6 kJ/mol) is 14 ± 8 kJ/mol lower in energy than dehydration of H^+(AsnGly) (117 ± 6 kJ/mol). The analogous TSs are very similar and correspond to similar vibrational motions, and ring formation again occurs at an atom adjacent to the methyl substitution site. This proximity suggests that a combination of inductive and possibly steric effects associated with the differing side chain leads to the changes observed.

Comparison to IRMPD Studies of H^+(AsnAla) and H^+(AsnVal)

Kempkes et al. have examined the dissociation products of H^+(AsnAla) in an infrared multiple photon dissociation (IRMPD) spectroscopic study [11] and characterized structures of the deamidation products formed, finding a combination of the succinimide and furanone complexes, although with an unknown branching ratio. Although they did not examine the reaction pathways, they did calculate product energies at the MP2(full)/6-311+G(2d,2p)//B3LYP/6-31++G(d,p) level of theory and obtained values that compare well with those reported in our current study. We find the H^+(AMEA-Suc) product is 22–52 kJ/mol lower in energy than H^+(AMA-Fur) across all levels of theory, which compares well with ~40 kJ/mol reported by Kempkes et al. More critical to the product formation is our present analysis of key TSs along the respective reaction coordinates, which indicate that the furanone product is favored by 14–32 kJ/mol. As discussed above, this analysis is consistent with the competitive nature of these two pathways.

Likewise, H^+(AsnAla) dehydration products formed were also characterized via IRMPD spectroscopy [43], and again, two product isomers were observed. Parallel to our current findings, a protonated oxazolone structure was identified, H^+(APAM-Oxa), where this structure dissociated via decarbonylation (consistent with its sequential loss identified in Scheme 2). Interestingly, a protonated diketopiperazine (DKP) structure was also observed, characterized by the sequential loss of ammonia (forming *m/z* 169, a dissociation channel not observed at high mass-resolution in the current TCID study but was observed by SORI-CID, Figure 2). In the current study, we located key reaction species leading to the DKP structure with rate-limiting energies 98–124 kJ/mol higher in energy than oxazolone formation (Figure S7). Thus, in the current TCID experiments, oxazolone formation would dominate at threshold energies, although contributions from DKP formation could occur at high collision energies. Given

the relatively high energies required for DKP formation, the possibility of this pathway contributing to the dehydration channel was not considered in our cross-section modeling.

Interestingly, behavior of the deamidation channel was different in the IRMPD analysis of H^+(AsnVal) [8]. Here, Kempkes et al. found that deamidation yields *exclusively* a furanone product. Their spectroscopic results are consistent with theoretical predictions (performed at the same level as the present theoretical work), where all levels of theory suggest that furanone formation is lower in energy than succinimide formation. Because the mechanisms of both pathways are not strongly influenced by the side chain, the pathways located in that study parallel those described here. Notably, at the MP2 level of theory (which predicts the competitive nature of the two furanone and succinimide pathways well), furanone formation was found to be 7 kJ/mol lower in energy than succinimide formation, 4 kJ/mol higher than the difference observed in the current theoretical analysis. Thus, the competitive nature of the alternative succinimide formation was disfavored by the Val side chain. On the basis of these results, furanone formation appears to be favored as the size of an aliphatic side chain increases, a hypothesis consistent with solution-phase studies [4] (where solution-phase kinetics find that $n + 1$ residues of Gly, Ala, and Val result in deamidation rates leading to succinimide intermediates of about 1, 25, and 253 days [6]) and one that could be tested by further gas-phase studies with AsnIle and AsnLeu.

Comparison to Solution-Phase Studies

Solution-phase studies have evaluated the effects of factors such as viscosity, pH, and ionic strength on the deamidation processes of asparagine and glutamine residues [4, 44]. Such studies provide valuable information regarding how these factors affect deamidation processes, with an overview of the likely solution-phase reactions given in Scheme 1. However, the characterization of important elementary steps in the solution phase becomes difficult because the complexities of solvation make it more difficult to isolate elementary steps in the reaction mechanism. Thus, it is particularly important to understand the relationship between gas-phase (which eliminates solvent effects) and solution-phase analyses of biological systems.

To evaluate how solvent might mediate the decompositions observed experimentally, the rate-limiting TSs for the proposed deamidation mechanisms detailed in this work were additionally optimized with the addition of one explicit water molecule (in the interests of computational time) embedded in a polar environment by use of the self-consistent reaction field (SCRF) theory [45]. Geometry optimizations were conducted at the B3LYP/6-311+G(d,p) level of theory. Single point energies using the polarizable continuum model (PCM) were calculated at the B3LYP, B3P86, and MP2 (full) levels of theory using a 6-311+G(2d,2p) basis set. The relative energies for these solvated species leading to furanone (the experimentally determined deamidation product) and succinimide (via a tetrahedral intermediate, predicted as a major pathway yielding succinimide structures in solution) [46] formation are given in Figure 8.

The relative energies of $TS_{N\text{-}Fur}$ (H_2O) change considerably compared to the non-solvated TS, increasing by 32–41 kJ/mol, comparable to a 36–38 kJ/mol increase observed in the H^+(AsnGly) study [7]. In both cases, the increase in energy is reasonable because the rate-limiting TS does not involve a proton transfer, but is rather characterized by concerted bond rupture and cyclization. Thus, the energy increases because the water only stabilizes the NH_3^+ moiety in both dipeptide systems. Given the similar mode of concerted bond rupture and cyclization, the rate-limiting TS for the succinimide pathway ($TS_{N\text{-}Suc}$) would likely observe a similar degree of increased energy, as observed explicitly in H^+(AsnGly), where the increase was 14–20 kJ/mol [7].

For succinimide formation via the tetrahedral intermediate, the relative energies of the rate-limiting TS *decrease* by 77, 82, and 73 kJ/mol at the B3LYP, B3P86, and MP2 levels of theory,

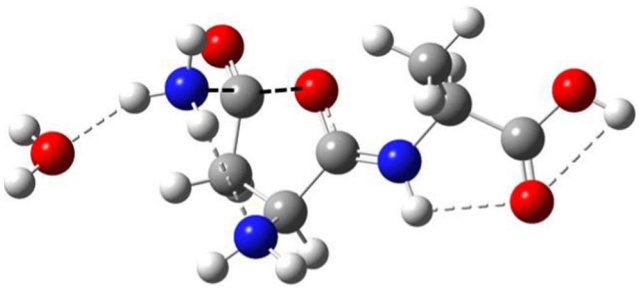

$TS_{N\text{-}Fur}(H_2O)$

(167.9, 170.9, 162.6)

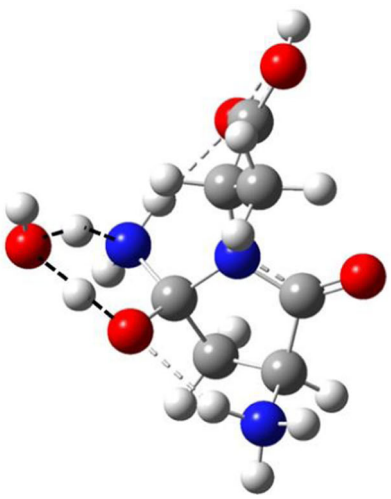

$TS_{N\text{-}Tet}(H_2O)$

(180.1, 147.4, 129.0)

Figure 8. Optimized structures for the solvated TSs for two of the proposed deamidation pathways, calculated at the B3LYP/6-311+G(d,p) level. Hydrogen bonds are indicated by gray dashed lines. Black dashed lines indicate bonds being broken or formed. Relative energies (kJ/mol) are indicated at the B3LYP, B3P86, and MP2 levels of theory, respectively

respectively. A similar decrease was found in our previous study of H^+(AsnGly) [7] and this decrease is comparable, although slightly larger, to the water solvation effects calculated by Catak and co-workers in a model asparagine residue [46]. Because this TS is characterized by concerted motions of two proton transfers, the added water molecule can facilitate those transfers via a relay-type mechanism [47], thus actively participating in the reaction such that overall lower reaction energies are found. Note that at the B3P86 and MP2 levels, this TS is lower in energy than the two other pathways elucidated here, suggesting that the tetrahedral intermediate may be a viable pathway for deamidation in solution, as originally suggested by Capasso et al. [48].

Interestingly, solvation effects also appear to affect the relative energetics related to the side chain. $TS_{N\text{-}Fur}$ (H_2O) is *lower* in energy than the analogous TS for H^+(AsnGly) by 2–6 kJ/mol, whereas $TS_{N\text{-}Tet}$ (H_2O) exhibits an 8–13 kJ/mol increase with respect to its analogous TS for H^+(AsnGly) [7]. Here, these results for furanone formation parallel our gas-phase trends, where predicted reaction energetics for furanone formation from H^+(AsnGly) and H^+(AsnAla) are nearly isoenergetic with each other. Thus, neither additional steric considerations nor water mediation appears to have a significant effect on the furanone reaction barrier. On the other hand, the predicted reaction energetics for succinimide formation are more consistent with trends found in solution. In the water-mediated cases, a side-chain steric argument is commonly invoked [4]; thus, the increase in energy observed for $TS_{N\text{-}Tet}$ (H_2O) compared to the analogous TS located in the H^+(AsnGly) study must be related to the methyl group of the Ala side chain.

Conclusions

H^+(AsnAla) decomposition was studied by measuring kinetic energy-dependent thresholds for collision-induced dissociation (TCID) with Xe using a GIBMS. From this analysis, 0 K threshold energies were determined and include consideration of the effects of reactant internal energy, multiple collisions with Xe, lifetime effects, and competition among channels. Complementary information was provided via SORI-CID upon collision with Ar using an FT-ICR MS where similar energetic behavior in ion intensities is observed in both analyses.

Our current analysis indicates that deamidation leading to H^+(AMA-Fur) formation is favored at threshold energies (123 ± 5 kJ/mol), with contributions from the succinimide product likely at higher energies, consistent with predicted reaction energies. Competitive modeling of the dehydration channel leads to a reaction threshold (103 ± 6 kJ/mol) that is lower by 20 kJ/mol than deamidation. The concomitant Ala and CO loss and sequential ammonia loss channels resulted in higher thresholds of 155 ± 7 and 291 ± 6 kJ/mol, respectively. All four channels are primarily limited by tight TSs. Overall, there is good agreement for all modeled primary channels between experimentally determined reaction energies and theoretical predictions, as shown by relatively low MADs (9–12 kJ/mol), with slightly larger MADs observed when the sequential channel was included (13–15 kJ/mol) at the B3LYP, B3LYP-GD3BJ, and MP2 levels of theory. The identification of key TSs and the experimentally determined threshold values here indicate that the deamidation process is energetically comparable to that observed previously in our study of H^+(AsnGly) decomposition. Theory indicates that the methyl side chain has an effect on the energetics of succinimide formation, but it does not significantly alter the energies for deamidation via the alternate furanone formation pathway.

We also determined, on a theoretical basis, the solvation effects associated with the addition of water to rate-limiting TSs yielding furanone and succinimide (via a tetrahedral intermediate) formation. Our results here parallel those found previously for H^+(AsnGly) [7], where solvation effects depend heavily on the specific motions of the key TSs involved. Specifically, a greater energetic cost is observed for TSs characterized by concerted motions of bond rupture and cyclization (furanone formation via $TS_{N\text{-}Fur}$ or succinimide formation via $TS_{N\text{-}Suc}$), rather than proton transfers (e.g., succinimide formation via $TS_{N\text{-}Tet}$) where a decrease in reaction energies is observed. Given that the accessibility to water molecules (via higher order structural effects) has been postulated as a key factor dictating reaction energetics [46], it would clearly be useful to extend these studies to larger systems allowing for the analysis of conformationally strained proteins that would have more limited access to water within the protein.

Overall, the results presented here identify the key elementary steps of the deamidation process of protonated asparaginyl alanine via the analysis of several competitive deamidation pathways. Analogous pathways were located when solvation effects were considered where we find that the correlation between unsolvated and solvated mechanisms is more complicated than assuming a general decrease in energy with the addition of water molecules. For future analyses, we hope to elucidate the effects of deamidation kinetics resulting from peptide length, sequence, and other higher order structural considerations, where continuing the study of solvated TSs should allow for the determination of key trends that bridge the gap between gas- and solution-phase studies.

Acknowledgements

The authors acknowledge support for this work by the National Science Foundation, Grants CHE-1664618 (PBA) and DBI-0922819 and CHE-1709789 (MTR). RRW also acknowledges support from Thomas C. Rumble Graduate Research and Summer Dissertation Fellowships at WSU. The authors gratefully acknowledge a grant of computer time from the Center for High Performance Computing at the University of Utah. Additionally, the authors acknowledge Marcus Tirado and Prof. Nicolas Polfer (Polfer Lab, University of Florida) for the synthesis of AsnAla used in the SORI experiments.

References

1. Walsh, C.T., Garneau-Tsodikova, S., Gatto, G.J.: Protein posttranslational modifications: the chemistry of proteome diversifications. Angew. Chem. Int. Ed. **44**, 7342–7372 (2005)
2. Mayer, S.E., Krebs, E.G.: Studies on the phosphorylation and activation of skeletal muscle phosphorylase and phosphorylase kinase in vivo. J. Biol. Chem. **245**, 3153–3160 (1970)
3. Deribe, Y.L., Pawson, T., Dikic, I.: Post-translational modifications in signal integration. Nat. Struct. Mol. Biol. **17**, 666–672 (2010)
4. Robinson, N.E., Robinson, A.B.: Molecular clocks: deamidation of asparaginyl and glutaminyl residues in peptides and proteins. Althouse Press, Cave Junction (2004)
5. Nilsson, M.R., Driscoll, M., Raleigh, D.P.: Low levels of asparagine deamidation can have a dramatic effect on aggregation of amyloidogenic peptides: implications for the study of amyloid formation. Protein Sci. **11**, 342–349 (2002)
6. Robinson, N.E., Robinson, A.B.: Molecular clocks. Proc. Natl. Acad. Sci. **98**, 944–949 (2001)
7. Boles, G.C., Wu, R.R., Rodgers, M.T., Armentrout, P.B.: Thermodynamics and mechanisms of protonated asparaginyl-glycine decomposition. J. Phys. Chem. B. **120**, 6525–6545 (2016)
8. Kempkes, L., Boles, G.C., Martens, J., Berden, G., Armentrout, P.B., Oomens, J.: Deamidation of protonated asparagine-valine investigated by a combined spectroscopic, guided ion beam, and theoretical study. J. Phys. Chem. A. **122**, 2424–2436 (2018)
9. Laskin, J., Byrd, M., Futrell, J.: Internal energy distributions resulting from sustained off-resonance excitation in FTMS. I. Fragmentation of the bromobenzene radical cation. Int. J. Mass Spectrom. **196**, 285–302 (2000)
10. Guo, X., Duursma, M.C., Al-Khalili, A., Heeran, R.M.A.: Experimental calibration of the SORI-CID internal energy scale: energy uptake and loss. Int. J. Mass Spectrom. **225**, 71–82 (2003)
11. Kempkes, L.J.M., Martens, J.K., Grzetic, J., Berden, G., Oomens, J.: Deamidation reactions of asparagine- and glutamine-containing dipeptides investigated by ion spectroscopy. J. Am. Soc. Mass Spectrom. **27**, 1855–1869 (2016)
12. Ervin, K.M., Armentrout, P.B.: Translational energy dependence of $Ar^+ + XY \rightarrow ArX^+ + Y$ ($XY = H_2$, D_2, HD) from thermal to 30 eV C.M. J. Chem. Phys. **83**, 166–189 (1985)
13. Muntean, F., Armentrout, P.B.: Guided ion beam study of collision-induced dissociation dynamics: integral and differental cross sections. J. Chem. Phys. **115**, 1213–1228 (2001)
14. Armentrout, P.B.: Not just a structural tool: the use of guided ion beam tandem mass spectrometry to determine thermochemistry. J. Am. Soc. Mass Spectrom. **13**, 419–434 (2002)
15. Moision, R.M., Armentrout, P.B.: An electrospray ionization source for thermochemical investigation with the guided ion beam mass spectrometer. J. Am. Soc. Mass Spectrom. **18**, 1124–1134 (2007)
16. Kim, T., Tolmachev, A.V., Harkewicz, R., Prior, D.C., Anderson, G., Udseth, H.R., Smith, R.D., Bailey, T.H., Rakov, S., Futrell, J.H.: Design and implementation of a new electrodynamic ion funnel. Anal. Chem. **72**, 2247–2255 (2000)
17. Heaton, A.L., Armentrout, P.B.: Thermodynamics and mechanism of the deamidation of sodium-bound asparagine. J. Am. Chem. Soc. **130**, 10227–10232 (2008)
18. Ye, S.J., Armentrout, P.B.: Absolute thermodynamic measurements of alkali metal cation interactions with a simple dipeptide and tripeptide. J. Phys. Chem. A. **112**, 3587–3596 (2008)
19. Heaton, A.L., Armentrout, P.B.: Thermodynamics and mechanism of protonated asparagine decomposition. J. Am. Soc. Mass Spectrom. **20**, 852–866 (2009)
20. Carpenter, J.E., McNary, C.P., Furin, A., Sweeney, A.F., Armentrout, P.B.: How hot are your ions really? A threshold collision-induced dissociation study of substituted benzylpyridium "thermometer" ions. J. Am. Soc. Mass Spectrom. **28**, 1876–1888 (2017)
21. Teloy, E., Gerlich, D.: Integral cross sections for ion-molecule reactions. 1. The guided beam technique. Chem. Phys. **4**, 417–427 (1974)
22. Gerlich, D.: Inhomogeneous RF fields: a versatile tool for the study of processes with slow ions. Adv. Chem. Phys. **82**, 1–176 (1992)
23. Aristov, N., Armentrout, P.B.: Collision-induced dissociation of vanadium monoxide ion. J. Phys. Chem. **90**, 5135–5140 (1986)
24. Dalleska, N.F., Honma, K., Sunderlin, L.S., Armentrout, P.B.: Solvation of transition metal ions by water. Sequential binding energies of $M^+(H_2O)_x$ (x = 1-4) for M = Ti - Cu determined by collision-induced dissociation. J. Am. Chem. Soc. **116**, 3519–3528 (1994)
25. Daly, N.R.: Scintillation type mass spectrometer ion detector. Rev. Sci. Instrum. **31**, 264–267 (1960)
26. Beyer, T.S., Swinehart, D.F.: Number of multiply-restricted partitions. Commun. ACM. **16**, 379 (1973)
27. Stein, S.E., Rabinovich, B.S.: On the use of exact state counting methods in RRKM rate calculations. Chem. Phys. Lett. **49**, 183–188 (1977)
28. Stein, S.E., Rabinovitch, B.S.: Accurate evaluation of internal energy level sums and densities including anharmonic oscillators and hindered rotors. J. Chem. Phys. **58**, 2438–2445 (1973)
29. Gilbert, R.G., Smith, S.C.: Theory of Unimolecular and Recombination Reactions. Blackwell Scientific, London (1990)
30. Robinson, P.J., Holbrook, K.A.: Unimolecular reactions. Wiley Interscience, New York (1972)
31. Rodgers, M.T., Ervin, K.M., Armentrout, P.B.: Statistical modeling of collision-induced dissociation thresholds. J. Chem. Phys. **106**, 4499–4508 (1997)
32. Rodgers, M.T., Armentrout, P.B.: Statistical modeling of competitive threshold collision-induced dissociation. J. Chem. Phys. **109**, 1787–1800 (1998)
33. Armentrout, P.B.: Statistical modeling of sequential collision-induced dissociation. J. Chem. Phys. **126**, 234302 (2007)
34. Hales, D.A., Lian, L., Armentrout, P.B.: Collision-induced dissociation of Nb_n^+ (n = 2-11): bond energies and dissociation pathways. Int. J. Mass Spectrom. Ion Process. **102**, 269–301 (1990)
35. Frisch, M.J., Trucks, G.W., Schlegel, H.B., Scuseria, G.E., Robb, M.A., Cheeseman, J.R., Scalmani, G., Barone, V., Petersson, G.A., Nakatsuji, H., Li, X., Caricato, M., Marenich, A., Bloino, J., Janesko, B.G., Gomperts, R., Mennucci, B., Hratchian, H.P., Ortiz, J.V., Izmaylov, A.F., Sonnenberg, J.L., Williams-Young, D., Ding, F., Lipparini, F., Egidi, F., Goings, J., Peng, B., Petrone, A., Henderson, T., Ranasinghe, D., Zakrzewski, V.G., Gao, J., Rega, N., Zheng, G., Liang, W., Hada, M., Ehara, M., Toyota, K., Fukuda, R., Hasegawa, J., Ishida, M., Nakajima, T., Honda, Y., Kitao, O., Nakai, H., Vreven, T., Throssell, K., Montgomery Jr., J.A., Peralta, J.E., Ogliaro, F., Bearpark, M., Heyd, J.J., Brothers, E., Kudin, K.N., Staroverov, V.N., Keith, T., Kobayashi, R., Normand, J., Raghavachari, K., Rendell, A., Burant, J.C., Iyengar, S.S., Tomasi, J., Cossi, M., Millam, J.M., Klene, M., Adamo, C., Cammi, R., Ochterski, J.W., Martin, R.L., Morokuma, K., Farkas, O., Foresman, J.B., Fox, D.J.: *Gaussian 09*. Revision D.01. Gaussian, Inc., Wallingford (2009)
36. Kesharwani, M.K., Brauer, B., Martin, J.M.L.: Frequency and zero-point vibrational energy scale factors for double-hybrid density functionals (and other selected methods): can anharmonic force fields be avoided? J. Phys. Chem. A. **119**, 1701–1714 (2015)
37. Fadda, E., Woods, R.J.: Contribution of the empirical dispersion correction on the conformation of short alanine peptides obtained by gas-phase QM calculations. Can. J. Chem. **91**, 859–865 (2013)
38. Yalcin, T., Khouw, C., Csizmadia, I.G., Peterson, M.R., Harrison, A.G.: Why are b ions stable species in peptide spectra? J. Am. Soc. Mass Spectrom. **6**, 1165–1174 (1995)
39. Paizs, B., Lendvay, G., Vekey, K., Suhai, S.: Formation of b_2^+ ions from protonated peptides: an ab initio study. Rapid Commun. Mass Spectrom. **13**, 525–533 (1999)
40. Harrison, A.G., Csizmadia, I.G., Tang, T.-H.: Structure and fragmentation of b_2 ions in peptide mass spectra. J. Am. Soc. Mass Spectrom. **11**, 427–436 (2000)
41. Konuklar, F.A., Aviyente, V., Sen, T.Z., Bahar, I.: Modeling the deamidation of asparagine residues via succinimde intermediates. J. Mol. Model. **7**, 147–160 (2001)
42. Muntean, F., Heumann, L., Armentrout, P.B.: Modeling kinetic shifts in threshold collision-induced dissociation. Case study: dichlorobenzene cation dissociation. J. Chem. Phys. **116**, 5593–5602 (2002)
43. Kempkes, L.J.M., Martens, J., Berden, G., Oomens, J.: Dehydration reactions of protonated dipeptides containing asparagine or glutamine investigated by infrared ion spectroscopy. Int. J. Mass Spectrom. **429**, 90–100 (2017)
44. Tyler-Cross, R., Schirch, V.: Effects of amino acid sequence, buffers, and ionic strength on the rate and mechanism of deamidation of asparagine residues in small peptides. J. Biol. Chem. **266**, 22549–22556 (1991)
45. Tapia, O., Goscinski, O.: Self-consistent reaction field theory of solvent effects. Mol. Phys. **29**, 1653–1661 (1975)

46. Catak, S., Monard, G., Aviyente, V., Ruiz-Lopez, M.F.: Reaction mechanism of deamidation of asparaginyl residues in peptides: effect of solvent molecules. J. Phys. Chem. A. **110**, 8354–8365 (2006)
47. Campbell, S., Rodgers, M.T., Marzluff, E.M., Beauchamp, J.L.: Deuterium exchange reactions as a probe of biomolecule structure. Fundamental studies of gas phase H/D exchange reactions of protonated glycine oligomers with D_2O, CD_3OD, CD_3CO_2D, and ND_3. J. Am. Chem. Soc. **117**, 12840–12854 (1995)
48. Capasso, S., Mazzarella, L., Sica, F., Zagari, A., Salvadori, S.: Kinetics and mechanism of succinimide ring formation in the deamidation process of asparagine residues. J. Chem. Soc. Perkin Trans. **2**, 679–682 (1993)